CHALMERS
FINITE ELEMENT CENTER

PREPRINT 2003–14

Nitsche's method combined with space–time finite elements for ALE fluid–structure interaction problems

Peter Hansbo, Joakim Hermansson, and Thomas Svedberg

Chalmers Finite Element Center
CHALMERS UNIVERSITY OF TECHNOLOGY
Göteborg Sweden 2003

CHALMERS FINITE ELEMENT CENTER

Preprint 2003–14

Nitsche's method combined with space–time finite elements for ALE fluid–structure interaction problems

Peter Hansbo, Joakim Hermansson, and Thomas Svedberg

CHALMERS

Chalmers Finite Element Center
Chalmers University of Technology
SE–412 96 Göteborg Sweden
Göteborg, September 2003

Nitsche's method combined with space–time finite elements for ALE fluid–structure interaction problems
Peter Hansbo, Joakim Hermansson, and Thomas Svedberg
NO 2003–14
ISSN 1404–4382

Chalmers Finite Element Center
Chalmers University of Technology
SE–412 96 Göteborg
Sweden
Telephone: +46 (0)31 772 1000
Fax: +46 (0)31 772 3595
www.phi.chalmers.se

Printed in Sweden
Chalmers University of Technology
Göteborg, Sweden 2003

NITSCHE'S METHOD COMBINED WITH SPACE–TIME FINITE ELEMENTS FOR ALE FLUID–STRUCTURE INTERACTION PROBLEMS

PETER HANSBO, JOAKIM HERMANSSON, AND THOMAS SVEDBERG

Abstract. We propose a weak method for handling the fluid-structure interface in finite element fluid-structure interaction based on Nitsche's method [14]. We assume transient incompressible Newtonian flow and, for the structure, undamped linear elasticity. For the time-discretization, we use the time-continuous (energy conserving) Galerkin method for the structure, and for the fluid we employ the time-discontinuous Galerkin method. This means that the velocity becomes piecewise constant on each timestep for the fluid, matching the time-derivative of the displacements in the solid which is also piecewise constant over a time step. We formulate the method and report some numerical examples using space-time oriented elements for the fluid in order to mimic Lagrangian or ALE-type simulations.

1. Introduction

In the simulation of Fluid-Structure Interaction (FSI), the coupling between the fluid and the structure is usually handled using partitioned methods, where different codes are used for the different physical domains, see, e.g., [5, 13, 15]. There are advantages to this approach, most prominently that different codes can be used for the different problems of solid and fluid modeling. On the other hand, since the solution procedure basically becomes a fixed point iteration scheme, the overall efficiency may not be the best [12]. In any case, the problem of how to couple motion and ensure equilibrium across the interface between the fluid and solid domains has to be addressed. This can be done by interpolating quantities from one mesh to the other as in [5], which is easiest if the approach is viewed as partitioned already at the outset, or by matching unknowns at the interface [12], which requires matching meshes, or, perhaps most conveniently, by means of Lagrange multiplier techniques [1, 4, 15]. It is, however, well known that Lagrange multipliers may be unstable if the relation between the discretization of the continua and the discretization of the multipliers is not chosen correctly, cf. [3]. Thus, it is not clear how to formulate a general Lagrange multiplier approach, in particular in view of the fact that the fluid mesh typically must be allowed to move relative to the structure mesh.

Peter Hansbo, Department of Applied Mechanics, Chalmers University of Technology, S–412 96 Göteborg, Sweden, *email*: hansbo@solid.chalmers.se

Joakim Hermansson, Department of Applied Mechanics, Chalmers University of Technology, S–412 96 Göteborg, Sweden, *email*: herman@solid.chalmers.se

Thomas Svedberg, Department of Applied Mechanics, Chalmers University of Technology, S–412 96 Göteborg, Sweden, *email*: hansbo@thsv.chalmers.se.

The aim of this paper is to propose a general, globally coupled, approach by means of the consistent weak coupling method originally proposed by Nitsche [14] for handling Dirichlet boundary conditions. This method is optimally convergent, stable, and can handle non-matching meshes, as was shown by Becker, Hansbo & Stenberg [2], where the case of coupling non-matching meshes for the solution of Poisson's equation was considered. Other recent applications of this approach include the elasticity problem with imperfect bonding on the interface [6], and the acoustic FSI problem [10].

In standard ALE formulations, the velocities are approximated using fixed (time-independent) basis functions. The ALE equations are then solved in a *fixed* domain at a given time, say the end of a given timestep. The mesh and velocities are updated in an iterative loop. In contrast, the space–time finite element method we use implies that the velocities are approximated using time-dependent basis functions, and the equations, which are retained in their Eulerian form, are integrated over the whole of the timestep (as opposed to a fixed time). We believe that this approach is conceptually much simpler: it is the space–time that is meshed and the ALE effect is achieved simply by the inclination of the elements in space–time. A particular feature of our approach is that the mesh geometry is tied to the approximation. This can be understood from the following argument. In a purely Lagrangian approach, the nodes will follow the path given by the computed velocity field. In the present paper, we will use a piecewise constant temporal approximation (along the paths), though higher order elements are of course possible. The relation between the velocity $\boldsymbol{v}_{\mathrm{F}}$ and the Lagrangian particle paths $\boldsymbol{x}(t)$ is given by the ODE $\boldsymbol{v}_{\mathrm{F}} = d\boldsymbol{x}/dt$, and thus it is natural that the geometry should vary linearly in time whenever the velocity is constant. Thus our approach relies heavily on finite element technology: isoparametric maps in space and a superparametric map in time from a reference element. In a standard ALE formulation the particle paths are typically approximated by solving the ODE using finite difference technology. Some benefits of using the space–time approach are:

- Clear conservation properties due to the variational framework (cf. [18])
- Conceptual simplicity; finite element techology is used both in space and time
- Streamline diffusion stabilization in space–time allows for simple finite element combinations for velocity and pressure

The main drawback is the restriction to finite elements in time. Two basic possibilities exist: discontinuous Galerkin, (used for the fluid in the current work) and time-continuous Galerkin methods (used for the structure in the current work). Here, a standard ALE implementation has a larger freedom of choice, which however comes at a price considering possible stability issues.

2. Problem formulation

We shall consider the fluid-structure interaction problem described by linear elasticity coupled with a viscous incompressible fluid; more precisely the case when the fluid is contained inside the elastic structure, possibly with a free surface. The domain Ω_{S} denotes the solid domain, with boundary composed of $\partial\Omega_{\mathrm{S}} = \Gamma \cup \partial\Omega_{\mathrm{S}}^{\mathrm{N}} \cup \partial\Omega_{\mathrm{S}}^{\mathrm{D}}$, where Γ is the interface separating the solid and fluid domains, $\partial\Omega_{\mathrm{S}}^{\mathrm{N}}$ is the part of the boundary where tractions are prescribed, and $\partial\Omega_{\mathrm{S}}^{\mathrm{D}}$ is the part of the boundary where displacements are prescribed. Analogously, we use the notation Ω_{F} and $\partial\Omega_{\mathrm{F}} = \Gamma \cup \partial\Omega_{\mathrm{F}}^{\mathrm{N}} \cup \partial\Omega_{\mathrm{F}}^{\mathrm{D}}$ for the fluid domain.

Given the body forces $\boldsymbol{f}_{\mathrm{S}}$, $\boldsymbol{f}_{\mathrm{F}}$ and densities ρ_{S}, ρ_{F}, we seek the displacement field $\boldsymbol{u}_{\mathrm{S}}$ in the solid and the velocity field $\boldsymbol{v}_{\mathrm{F}}$ and pressure p in the fluid, obeying the relations

$$\rho_{\mathrm{F}}\frac{\partial \boldsymbol{v}_{\mathrm{F}}}{\partial t} + \rho_{\mathrm{F}}\boldsymbol{v}_{\mathrm{F}}\cdot\nabla\boldsymbol{v}_{\mathrm{F}} - \nabla\cdot\boldsymbol{\sigma}(\boldsymbol{v}_{\mathrm{F}},p) = \boldsymbol{f}_{\mathrm{F}} \quad \text{in } \Omega_{\mathrm{F}}, \tag{2.1}$$

$$\nabla\cdot\boldsymbol{v}_{\mathrm{F}} = 0 \quad \text{in } \Omega_{\mathrm{F}}, \tag{2.2}$$

$$\rho_{\mathrm{S}}\frac{\partial^2 \boldsymbol{u}_{\mathrm{S}}}{\partial t^2} - \nabla\cdot\boldsymbol{\sigma}(\boldsymbol{u}_{\mathrm{S}}) = \boldsymbol{f}_{\mathrm{S}} \quad \text{in } \Omega_{\mathrm{S}}, \tag{2.3}$$

$$\boldsymbol{n}\cdot\boldsymbol{\sigma}(\boldsymbol{u}_{\mathrm{S}}) - \boldsymbol{n}\cdot\boldsymbol{\sigma}(\boldsymbol{v}_{\mathrm{F}},p) = \mathbf{0} \quad \text{on } \Gamma, \tag{2.4}$$

$$\boldsymbol{v}_{\mathrm{F}} - \frac{\partial \boldsymbol{u}_{\mathrm{S}}}{\partial t} = 0 \quad \text{on } \Gamma, \tag{2.5}$$

$$\boldsymbol{u}_{\mathrm{S}} = \mathbf{0} \quad \text{on } \partial\Omega_{\mathrm{S}}^{\mathrm{D}} \tag{2.6}$$

$$\boldsymbol{v}_{\mathrm{F}} = \mathbf{0} \quad \text{on } \partial\Omega_{\mathrm{F}}^{\mathrm{D}} \tag{2.7}$$

$$\boldsymbol{n}\cdot\boldsymbol{\sigma}(\boldsymbol{u}_{\mathrm{S}}) = \mathbf{0} \quad \text{on } \partial\Omega_{\mathrm{S}}^{\mathrm{N}} \tag{2.8}$$

$$\boldsymbol{n}\cdot\boldsymbol{\sigma}(\boldsymbol{v}_{\mathrm{F}},p) = \mathbf{0} \quad \text{on } \partial\Omega_{\mathrm{F}}^{\mathrm{N}} \tag{2.9}$$

Here, the components of the stress tensor in the solid are given by

$$\sigma_{ij} = \lambda\,\delta_{ij}\nabla\cdot\boldsymbol{u}_{\mathrm{S}} + 2\mu\,\varepsilon_{ij}\left(\boldsymbol{u}_{\mathrm{S}}\right),$$

where δ_{ij} is the Kronecker delta,

$$\varepsilon_{ij}(\boldsymbol{u}) = \frac{1}{2}\left(\frac{\partial u_i}{\partial x_j} + \frac{\partial u_j}{\partial x_i}\right),$$

and λ and μ are the Lamé constants. In the fluid, we have

$$\sigma_{ij} = 2\mu_{\mathrm{F}}\varepsilon_{ij}\left(\boldsymbol{v}_{\mathrm{F}}\right) - p\delta_{ij}.$$

In case the fluid can slip along Γ, the continuity of the traction on Γ is replaced by continuity of normal stresses $\sigma_n := \boldsymbol{n}\cdot(\boldsymbol{\sigma}\cdot\boldsymbol{n})$, and continuity of velocity by continuity of normal velocity. We have let $\boldsymbol{n}$ denote the outward pointing normal to Ω_{F} on the interface Γ that separates Ω_{F} from Ω_{S} as well as the outward pointing normal on the traction boundaries. Equations (2.1)–(2.2) describe the incompressible Navier-Stokes equations; (2.3) is the vibration problem of linearized elasticity; (2.4) signifies continuity of tractions; (2.5) continuity of velocity; (2.6)–(2.7) are the displacement/velocity boundary conditons; (2.8)–(2.9) are the traction-free boundaries.

We emphasize that we assume small deformations in the solid, so we do not make a distinction between material and spatial time derivatives for the solid.

3. The space-time finite element formulation

In order to define the finite element form of the fluid–structure problem, we first introduce some notations.

The time interval $0 \leq t \leq T$ is divided into N intervals I_k as

$$I_k = (t_k, t_{k+1}],$$

where $0 = t_0 < t_1 < \ldots < t_N = T$. Let V_k^h denote the spatial finite element space associated with the time interval I_k (possibly different at different intervals) and defined by

$$V_k^h = \{v(\boldsymbol{x}) : v \text{ is continuous and linear in } \boldsymbol{x} \text{ on each triangle}\}.$$

We introduce the *mesh velocity* $\boldsymbol{\beta}_k \in V_k^h$ and let the mesh alignment lines $\boldsymbol{x}_k(t)$ be given by equation

$$\boldsymbol{x}_k(t) = \boldsymbol{x}(t_k) + (t - t_k)\boldsymbol{\beta}_k \quad \text{for } t \in I_k.$$

Now, for each I_k we define a space-time reference domain $\hat{S}_{\mathrm{F}}^k$ as

$$\hat{S}_{\mathrm{F}}^k = \Omega_{\mathrm{F}}(t_k) \times I_k.$$

and a map F_k by

$$(\boldsymbol{x}, t) = F_k(\boldsymbol{x}(t_k), t) = (\boldsymbol{x}_k(t), t).$$

The space-time FE spaces on the reference slab $\hat{S}_{\mathrm{F}}^k$ are defined as

$$\hat{V}^{hk}(\hat{S}_{\mathrm{F}}^k) = \{\hat{v} : \hat{v}(\boldsymbol{x}(t_k), t) = \hat{w}(\boldsymbol{x}_k) \in V_k^h\}$$

and for each function $\hat{v}(\boldsymbol{x}, t)$ we associate a function $v(\boldsymbol{x}, t)$ by $v(\boldsymbol{x}, t) = \hat{v}(\boldsymbol{x}(t_k), t)$ for $(\boldsymbol{x}, t) = F_k(\boldsymbol{x}(t_k), t)$. Then our finite element space can be written

$$V^{hk}(S^k) = \{v : v(\boldsymbol{x}, t) = \hat{v}(\boldsymbol{x}(t_k), t) \in \hat{V}^{hk}(\hat{S}_{\mathrm{F}}^k), (\boldsymbol{x}, t) = F_k(\boldsymbol{x}(t_k), t)\}.$$

The mesh alignment lines thus define the path a node is traveling in space-time, for instance, if the mesh is fixed in time then $\boldsymbol{\beta}_k = 0$ and the path is aligned along the time axis. In practice, the alignment defined by F_k is handled by standard superparametric mappings from a reference element, cf. [7]. We also note that the approximation is piecewise constant in time along the mesh lines. Thus if the mesh is allowed to move according to the computed velocities (a Lagrangian approach), then there is a perfect match with the linear map F_k and the convective derivative will vanish *exactly*. We emphasize that this does not have to be *assumed*; it is a consequence of our choice of approximation of the velocities and of the geometry of space–time.

For the structure part, for which we assume small deformations, the domain is fixed in space (see, however, Example 4.2) and the space–time domain can be directly divided into slabs $S_{\mathrm{S}}^k = \Omega_{\mathrm{S}} \times I_k$. The (fixed) space-time interface can be correspondingly divided into $S_{\mathrm{I}}^k = \Gamma \times I_k$. The finite element space we use is defined as

$$\begin{aligned} W^{hk}(\Omega_{\mathrm{S}}, t) = \{v(\boldsymbol{x}, t) : {} & v \text{ is continuous, piecewise linear in space,} \\ & \text{and linear in time on each } S_{\mathrm{S}}^k\}. \end{aligned}$$

The finite element formulation for the fluid–structure interaction problem can now be written: Find $\boldsymbol{V}_{\mathrm{F}} \in [V^{hk}]^d$, $d = 2$ or $d = 3$, $P \in V^{hk}$, $\boldsymbol{V}_{\mathrm{S}} \in [W^{hk}]^d$, and $\boldsymbol{U}_{\mathrm{S}} \in [W^{hk}]^d$ such that

$$
\begin{aligned}
&\int_{S_{\mathrm{F}}^k} \rho_{\mathrm{F}}\Big(\frac{\partial \boldsymbol{V}_{\mathrm{F}}}{\partial t} + \boldsymbol{V}_{\mathrm{F}} \cdot \nabla \boldsymbol{V}_{\mathrm{F}}\Big) \cdot \boldsymbol{\vartheta}_{\mathrm{F}} \,\mathrm{d}\Omega \mathrm{d}t - \int_{S_{\mathrm{F}}^k} P\, \nabla \cdot \boldsymbol{\vartheta}_{\mathrm{F}} \,\mathrm{d}\Omega \mathrm{d}t \\
&+2\mu \int_{S_{\mathrm{F}}^k} \boldsymbol{\varepsilon}(\boldsymbol{V}_{\mathrm{F}}) : \boldsymbol{\varepsilon}(\boldsymbol{\vartheta}_{\mathrm{F}}) \,\mathrm{d}\Omega \mathrm{d}t + \int_{S_{\mathrm{F}}^k} \nabla \cdot \boldsymbol{V}_{\mathrm{F}}\, q \,\mathrm{d}\Omega \mathrm{d}t + \rho_{\mathrm{F}} \int_{\Omega_{\mathrm{F}}(t_k)} (\boldsymbol{V}_{\mathrm{F}}^+ - \boldsymbol{V}_{\mathrm{F}}^-) \cdot \boldsymbol{\vartheta}_F^+ \,\mathrm{d}\Omega \\
&+ \int_{S_{\mathrm{F}}^k} \delta_1 \Big[\rho_{\mathrm{F}}\Big(\frac{\partial \boldsymbol{V}_{\mathrm{F}}}{\partial t} + \boldsymbol{V}_{\mathrm{F}} \cdot \nabla \boldsymbol{V}_{\mathrm{F}}\Big) + \nabla P\Big] \cdot \Big[\rho_{\mathrm{F}}\Big(\frac{\partial \boldsymbol{\vartheta}_{\mathrm{F}}}{\partial t} + \boldsymbol{V}_{\mathrm{F}} \cdot \nabla \boldsymbol{\vartheta}_{\mathrm{F}}\Big) + \nabla q\Big] \mathrm{d}\Omega \mathrm{d}t \\
&+\rho_{\mathrm{S}} \int_{S_{\mathrm{S}}^k} \dot{\boldsymbol{V}}_{\mathrm{S}} \cdot \dot{\boldsymbol{\vartheta}}_{\mathrm{S}} \,\mathrm{d}\Omega \mathrm{d}t + \int_{S_{\mathrm{S}}^k} \boldsymbol{\sigma}(\boldsymbol{U}_{\mathrm{S}}) : \boldsymbol{\varepsilon}(\dot{\boldsymbol{\vartheta}}_{\mathrm{S}}) \,\mathrm{d}\Omega \mathrm{d}t \\
&- \int_{S_{\mathrm{I}}^k} \boldsymbol{t}(\boldsymbol{V}_{\mathrm{F}}, P, \boldsymbol{U}_{\mathrm{S}}) \cdot (\boldsymbol{\vartheta}_{\mathrm{F}} - \dot{\boldsymbol{\vartheta}}_{\mathrm{S}}) \,\mathrm{d}\Gamma \mathrm{d}t - \int_{S_{\mathrm{I}}^k} \boldsymbol{t}(\boldsymbol{\vartheta}_{\mathrm{F}}, q, \boldsymbol{\vartheta}_{\mathrm{S}}) \cdot (\boldsymbol{V}_{\mathrm{F}} - \dot{\boldsymbol{U}}_{\mathrm{S}}) \,\mathrm{d}\Gamma \mathrm{d}t \qquad (3.1)\\
&+ \gamma \sum_{E \in S_{\mathrm{I}}^k} \int_E \frac{1}{h_E} (\boldsymbol{V}_{\mathrm{F}} - \dot{\boldsymbol{U}}_{\mathrm{S}}) \cdot (\boldsymbol{\vartheta}_{\mathrm{F}} - \dot{\boldsymbol{\vartheta}}_{\mathrm{S}}) \mathrm{d}\Gamma \mathrm{d}t \\
&= \int_{S_{\mathrm{F}}^k} \boldsymbol{f}_{\mathrm{F}} \cdot \boldsymbol{\vartheta}_{\mathrm{F}} \,\mathrm{d}\Omega \mathrm{d}t + \int_{S_{\mathrm{F}}^k} \delta_1 \boldsymbol{f}_{\mathrm{F}} \cdot \Big(\rho_{\mathrm{F}}\Big(\frac{\partial \boldsymbol{\vartheta}_{\mathrm{F}}}{\partial t} + \boldsymbol{V}_{\mathrm{F}} \cdot \nabla \boldsymbol{\vartheta}_{\mathrm{F}}\Big) + \nabla q\Big) \,\mathrm{d}\Omega \mathrm{d}t \\
&+ \int_{S_{\mathrm{S}}^k} \boldsymbol{f}_{\mathrm{S}} \cdot \dot{\boldsymbol{\vartheta}}_{\mathrm{S}} \,\mathrm{d}\Omega \mathrm{d}t
\end{aligned}
$$

and

$$
\int_{S_{\mathrm{S}}^k} (\boldsymbol{V}_{\mathrm{S}} - \dot{\boldsymbol{U}}_{\mathrm{S}}) \cdot \dot{\boldsymbol{\theta}}_{\mathrm{S}} \mathrm{d}\Omega \mathrm{d}t = 0 \qquad (3.2)
$$

for all $\boldsymbol{\vartheta}_{\mathrm{F}} \in [V^{hk}]^d, q \in V^{hk}$, $\boldsymbol{\vartheta}_{\mathrm{S}} \in [W^{hk}]^d$ and $\boldsymbol{\theta}_{\mathrm{S}} \in [W^{hk}]^d$. At time $t = 0$, $\boldsymbol{V}_{\mathrm{F}}^- = \boldsymbol{v}_{\mathrm{F}}(\boldsymbol{x}, 0)$. Further, the superscribed dot denotes time derivative. The stabilizing parameter δ_1 in the streamline diffusion method is given by $\delta_1 = C_1 \frac{1}{2} h/(1+|\boldsymbol{V}_{\mathrm{F}}|)$, see [7], where C_1 is a positive constant of $O(1)$. Further,

$$
\boldsymbol{v}^{\pm} = \lim_{s \to 0_{\pm}} \boldsymbol{v}(t_k + s).
$$

We note that the method is similar to a penalty-method, but with additional terms involving the traction vector, $\boldsymbol{t} := \boldsymbol{\sigma} \cdot \boldsymbol{n}$, on the interaction interface. This is in order to create a *consistent* method, i.e., one that holds with the exact solution inserted. The traction vector can be chosen as any convex combination of the traction on the fluid side and on the solid side, cf. [2]. Here, we choose to use the traction from the fluid side, which is in line with traditional approaches where forces are transferred from the fluid to the solid rather than vice versa. The (computable) parameter γ has to be chosen large enough for stability (obtaining a positive definite stiffness matrix), see [2]. In the numerical examples below, we have chosen this parameter considerably larger than this limit in order to avoid computing it and yet be on the safe side. The h_E on each interface element, which constitutes of two neighboring nodes in the interface, is given by $h_E = \max(2\frac{K_{\mathrm{F}}}{h_{\mathrm{F}}}, 2\frac{K_{\mathrm{S}}}{h_{\mathrm{S}}})$, where K_{F} and K_{S} are the element areas of the adjacent fluid and structural element to the the interface element, and h_{F} and h_{S} are the length of the fluid and the structural element sides on the interface.

The origins of the terms in (3.1) are as follows. The two first rows represent the left hand side of the weak form of the momentum equation for the fluid. The last term in the second row invokes the 'initial' velocity condition weakly at the bottom of the space-time slab, allowing for time–discontinuous fluid velocities. The third row contains the terms arising from the perturbation of the test functions according to the streamline diffusion method, as also the term on the right hand side including the parameter δ_1. In the fourth row we have the left hand side of the weak form of the structural momentum equation. The fluid–structure coupling is represented by the fifth and the sixth row, where the first term in the fifth row arises when then FE forms of the momentum equations for the fluid and the structure are added. Further, the second term in the fifth row and the γ-term in the sixth row are added terms according to Nitsche's method. The first term is added in order to symmetrize the approximation (of the viscous part), and the second term (penalty) is added to make the method stable. Finally, equation (3.2) is present since the structural momentum equations have been rewritten on first order form.

Choice of basis and test functions. Since the equations that describe the elastic structure in this work do not dissipate energy, we choose test functions that are of one order lower in time than the basis functions, corresponding to the time-continuous Galerkin method [8, 9]. The lowest order time-continuous Galerkin method is related to the Crank–Nicolson time stepping scheme [8], which is energy conserving (this quality holds also for higher order versions [9]).

With a piecewise linear approximation in time of the displacement field, the velocity (more precisely, the time derivative of the approximate displacement) becomes piecewise constant. This we match on the fluid side by employing the time-discontinuous Galerkin method for the fluid domain, using a piecewise constant time approximation of the velocity, which is closely related to backward Euler method. This is not crucial since the interface conditions are imposed weakly; in principle the discretization of the fluid and solid domains can be chosen independently in space as well as time.

4. Numerical examples

In the numerical examples the coupling is enforced weakly via the velocities according to the formulation in (3.1). The method does not, in its current form, take the deformation of the solid into account, since the elasticity equations are formulated by the small deformation assumption. The normal vector to the structural domain thus remains constant. However, if the elastic structure undergoes large rigid body translations (but not rotations), the geometry changes of the fluid domain can be taken into account also with this simple model, since the normal vector of the structure does not change during a rigid body translation. This is demonstrated in the second numerical example.

4.1. **A solitary wave encountering an elastic wall.** This example treats a solitary wave encountering an elastic wall, see Figure 1. The fluid is assumed to be inviscid and the density is given by $\rho_{\mathrm{F}} = 1\,\mathrm{kg/m}^3$. Further, the gravity is $g = 9.8\,\mathrm{m/s}^2$. The undisturbed domain has the dimensions $160 \times 10\,\mathrm{m}$ and the maximum elevation, H, of the starting wave is $2\,\mathrm{m}$. The (linear) elastic wall has the dimensions $1 \times 16\,\mathrm{m}$ and the following material data: $E = 10^7\,\mathrm{N/m}^2$, $\nu = 0.3$ and $\rho_{\mathrm{S}} = 10\,\mathrm{kg/m}^3$. Moreover, the fluid can slip on the rigid and elastic boundaries. This means that the coupling terms contain only the normal component of the traction. Thus the Nitsche terms in the FE formulation (3.1) can be written as

$$
\begin{aligned}
&-\int_{S_{\mathrm{I}}^k} \sigma_n(\boldsymbol{V}_{\mathrm{F}}, P, \boldsymbol{U}_{\mathrm{S}})(\boldsymbol{\vartheta}_{\mathrm{F}} - \dot{\boldsymbol{\vartheta}}_{\mathrm{S}})\cdot\boldsymbol{n}\,\mathrm{d}\Gamma\mathrm{d}t - \int_{S_{\mathrm{I}}^k} \sigma_n(\boldsymbol{\vartheta}_{\mathrm{F}}, q, \boldsymbol{\vartheta}_{\mathrm{S}})(\boldsymbol{V}_{\mathrm{F}} - \dot{\boldsymbol{U}}_{\mathrm{S}})\cdot\boldsymbol{n}\,\mathrm{d}\Gamma\mathrm{d}t \\
&+\gamma \sum_{E\in S_{\mathrm{I}}^k} \int_E \frac{1}{h_E}\big(\boldsymbol{n}\cdot(\boldsymbol{V}_{\mathrm{F}} - \dot{\boldsymbol{U}}_{\mathrm{S}})\big)\big((\boldsymbol{\vartheta}_{\mathrm{F}} - \dot{\boldsymbol{\vartheta}}_{\mathrm{S}})\cdot\boldsymbol{n}\big)\mathrm{d}\Gamma\mathrm{d}t.
\end{aligned}
$$

The starting wave and its velocity field, see Figure 2, is generated using Laitone's approximation, see, e.g., [16]. The velocities and the elevation, η, are according to Laitone's approximation given as

$$
\begin{aligned}
v_1 &= \sqrt{gd}\frac{H}{d}\mathrm{sech}^2\left((x_1 - ct)\sqrt{\frac{3H}{4d^3}}\right), \\
v_2 &= \sqrt{3gd}\left(\frac{H}{d}\right)^{3/2}\frac{x_2}{d}\mathrm{sech}^2\left((x_1 - ct)\sqrt{\frac{3H}{4d^3}}\right)\tanh\left((x_1 - ct)\sqrt{\frac{3H}{4d^3}}\right), \\
\eta &= H\mathrm{sech}^2\left((x_1 - ct)\sqrt{\frac{3H}{4d^3}}\right),
\end{aligned}
$$

where

$$
c = \sqrt{gd\left(1 + \frac{H}{d}\right)}.
$$

In the computations the nodes on the free surface are moved with the particle velocity, and the interior nodes the are moved using Laplacian smoothing. The coefficient in the stabilizing parameter in the streamline diffusion method is chosen as $C_1 = 0.01$. Further, the parameter in the coupling term is set to $\gamma = 10^4$. The fluid mesh contains 2298 elements and 1286 nodes, and the structural mesh contains 240 elements and 164 nodes. The time step is $0.02\,\mathrm{s}$. Further, the wall displacement at the initial state, see Figure 5, is computed using the static pressure.

The results are presented as follow: Snapshots of the starting wave and the wave when the wave crest reaches its maximum are depicted in Figure 2. The wave crest height versus

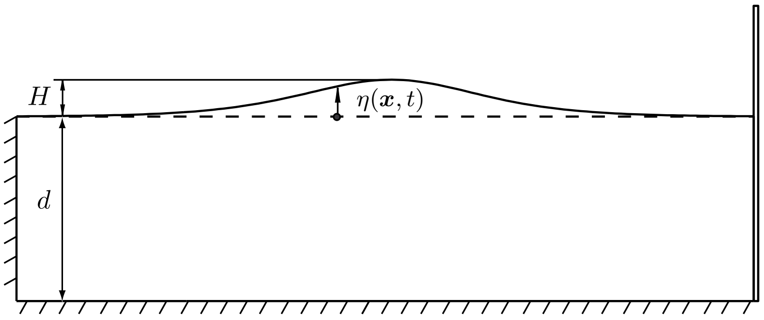

FIGURE 1. Initial computational domain.

time does not differ significantly in the presence of the elastic wall in comparison to a rigid wall, see Figure 3. The maximal wave heights occur at $t = 7.3\,\mathrm{s}$ and is 14.60 m for the rigid wall and 14.56 m for the elastic wall. The maximum pressures occur for both cases at $t = 7.14\,\mathrm{s}$, and are with the elastic wall and the rigid wall $132.8\,\mathrm{N/m^2}$ and $132.3\,\mathrm{N/m^2}$, respectively. The results obtained with the rigid wall can be compared with the results presented in [16], where the maximum wave height was 14.48 m and occured at 7.6 s. In Figure 4 the horizontal tip displacement and velocity of the elastic wall versus time are given. A spectral analysis of the tip displacement shows that the superimposed frequency, shown in Figure 4, is about 1.4 Hz. This value is close to the second eigenfrequency of the wall, which is 1.29 Hz. To verify that the excitation of the superimposed frequency is not due to an imbalance in the equilibrium at the interface at the initial state, we added damping during about a second, and as soon as the damping was released the superimposed frequency appeared again.

The lowest eigenfrequency of the wall is 0.034 Hz and the third is 9.5 Hz. Further, the wall displacement at maximum tip displacement is seen in Figure 5. To see how well the normal velocity coupling works, the normal velocities at the interface are plotted at two different times, see Figure 6. Note that the structural velocities at the interface are computed as $\dot{\boldsymbol{U}}_{\mathrm{S}} = (\boldsymbol{U}_{\mathrm{S}}^{k+1} - \boldsymbol{U}_{\mathrm{S}}^{k})/(t_{k+1} - t_k)$, since it is $\dot{\boldsymbol{U}}_{\mathrm{S}}$ that is included in the coupling terms, see (3.1). We conclude that the fluid flow is only marginally influenced by the appearance of the elastic wall with our choices of input data.

4.2. **Flow past a cylinder connected to an elastic spring.** In the second example, flow past a cylinder connected to a vertical elastic spring in a rectangular domain is simulated. In this example, the displacement of the solid domain is so large that its effect on the fluid domain has to be taken into account. Note, however, that we still use small deformation theory in the solid; thus, in all other respects it may still be considered fixed.

The domain has the dimensions $61 \times 32\,\mathrm{m}$, and the cylinder has the radius $r = 1\,\mathrm{m}$ and is positioned at $(16, 16)$. Constraints that hinder the cylinder to move in the x_1-direction are applied on two nodes. The fluid mesh has 3807 elements and 1986 nodes. The cylinder is modeled using 472 elements and 262 nodes. The structural nodes on the cylinder surface are positioned such that the structural and the fluid elements match on the interface.

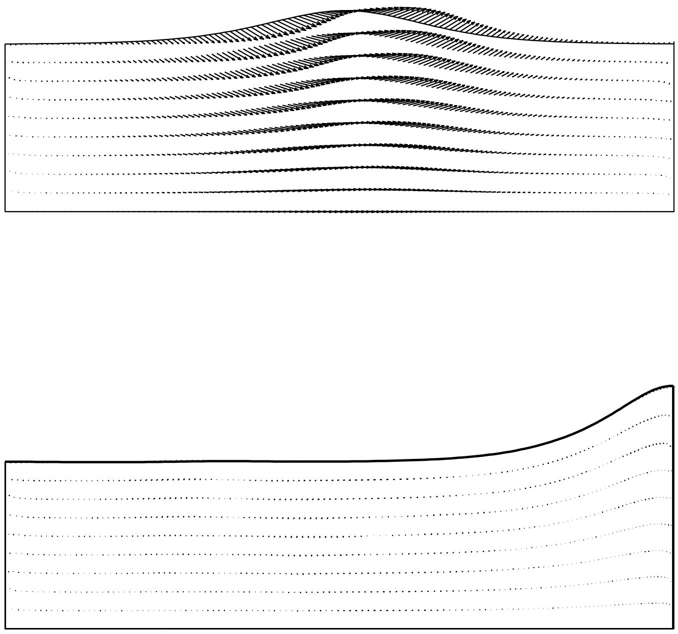

FIGURE 2. A solitary wave encountering an elastic wall. Start wave (top) and a snapshot at $t = 7.3\,\mathrm{s}$ (bottom). The vertical axis is exaggerated 4 times.

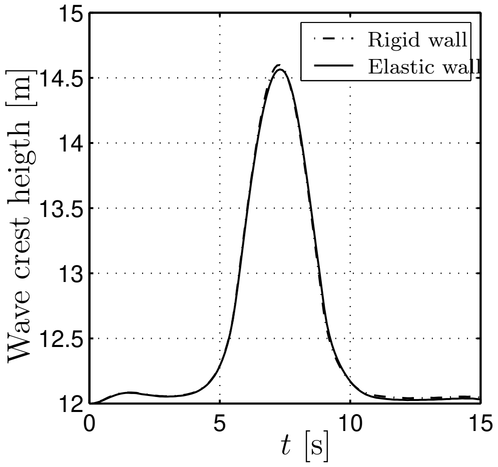

FIGURE 3. Wave crest height (measured from the bottom of the domain) versus time for a rigid and an elastic wall.

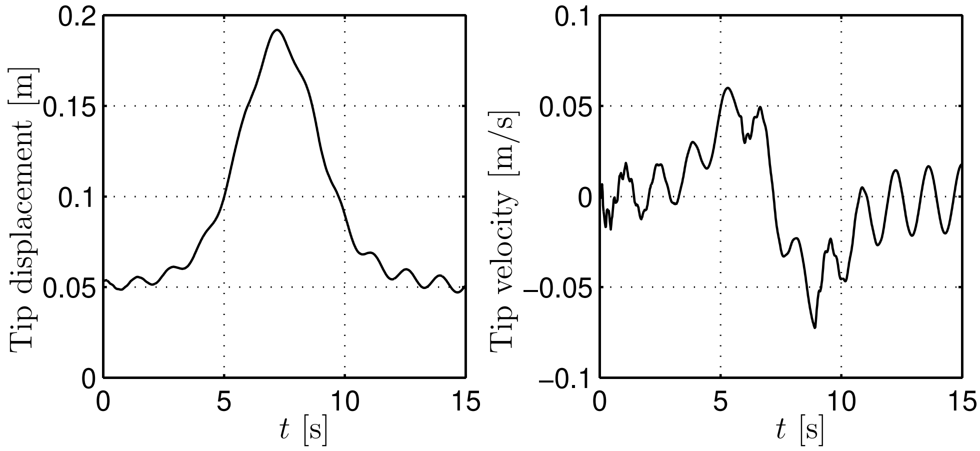

Figure 4. Tip displacement (left) and tip velocity (right) of the elastic wall versus time.

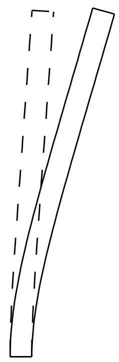

Figure 5. Wall displacement at initial state (dashed line) and at time $t = 7.3\,\mathrm{m}$ (solid line). Exaggerated 20 times.

Further, the coefficient in the streamline diffusion method is $C_1 = 1$, and the parameter in the coupling term is $\gamma = 10^6$. On the inflow boundary (the left) the velocities are prescribed as $\{v_1, v_2\} = \{1, 0\}\,\mathrm{m/s}$, and on the outflow boundary a traction-free condition is imposed. The no-slip condition is applied on the top and the bottom boundaries, and on the cylinder surface. Further, the coefficient of viscosity is $\mu_{\mathrm{F}} = 0.01\,\mathrm{kg/(ms)}$ and the density $\rho_{\mathrm{F}} = 1\,\mathrm{kg/m^3}$. The following structural input data are used: $\rho_{\mathrm{S}} = 1\,\mathrm{kg/m^3}$, Young's modulus $E = 2.1{\cdot}10^{11}\,\mathrm{N/m^2}$, Poisson's ratio $\nu = 0.3$, and the spring stiffness $k = 0.86\,\mathrm{N/m}$. These structural data give an eigenfrequency of $0.083\,\mathrm{Hz}$, which corresponds to a Strouhal number $\mathrm{St} = 0.166$. Further, plain strain was assumed.

In order to obtain a periodic solution, we first carry out a computation with a fixed cylinder. The Reynolds number $\mathrm{Re} = 100$ is used, defined as $\mathrm{Re} := \rho_{\mathrm{F}} V r/\mu_{\mathrm{F}}$, where V is the inflow velocity. The last part of the periodic results of the lift and drag coefficients

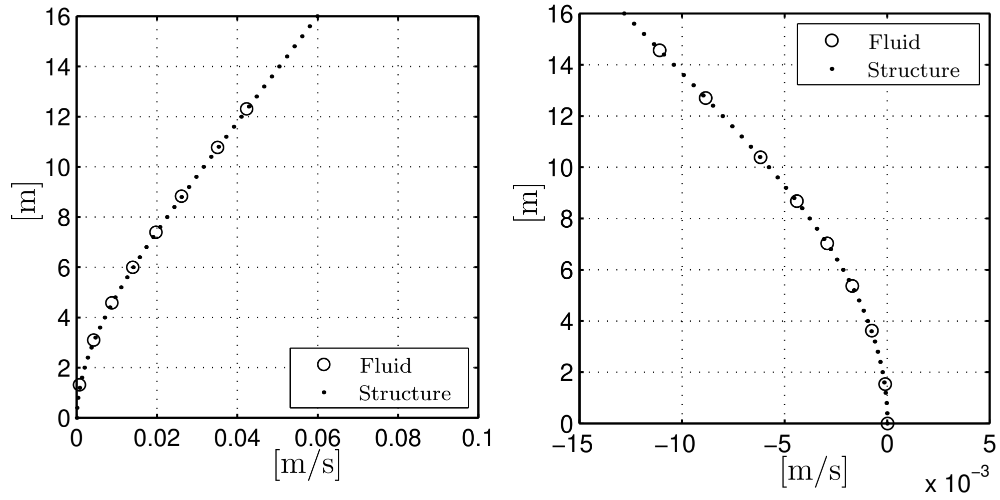

FIGURE 6. The normal velocity at the interface at at $t = 5.3\,\text{s}$ (left) and $t = 7.3\,\text{s}$ (right).

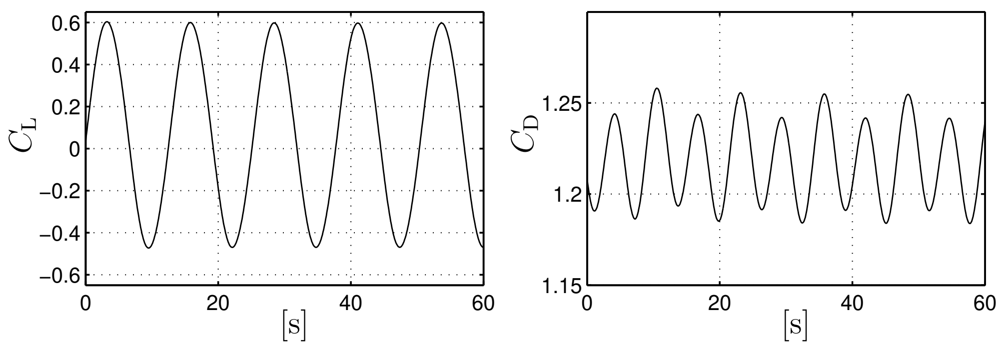

FIGURE 7. Lift (left) and drag (right) coefficients versus time for the fixed cylinder.

versus time can be seen in Figure 7. Note that the time scales are shifted to zero. The lift and drag coefficients are defined as $C_{\text{L}} = F_{\text{L}}/(\frac{1}{2}\rho_{\text{F}} V 2r)$ and $C_{\text{D}} = F_{\text{D}}/(\frac{1}{2}\rho_{\text{F}} V 2r)$, respectively, where F_{L} is the lift force and F_{D} is the drag force. The Strouhal number, $\text{St} := 2fr/V$, where f is the frequency of the vortices, is calculated to $\text{St} = 0.158$. This can be compared with $\text{St} = 0.167$ obtained in [17], where twice as many nodes were used.

In the simulation of the cylinder connected to the vertical spring, the solution from the fixed cylinder simulation at time $t = 0$ is used as a start solution, see Figure 10. The eigenfrequency of the spring mass system is $0.083\,\text{Hz}$, which is close the periodicity of the lift coefficient, namely $0.079\,\text{Hz}$. The lift coefficient at the initial state is $C_{\text{L}} = 0.034$. The vertical displacement and velocity of the cylinder versus time are seen in Figure 9, and the drag and lift coefficients are seen in Figure 8. Snapshots of the velocity field and the pressure at different times are seen in Figure 10.

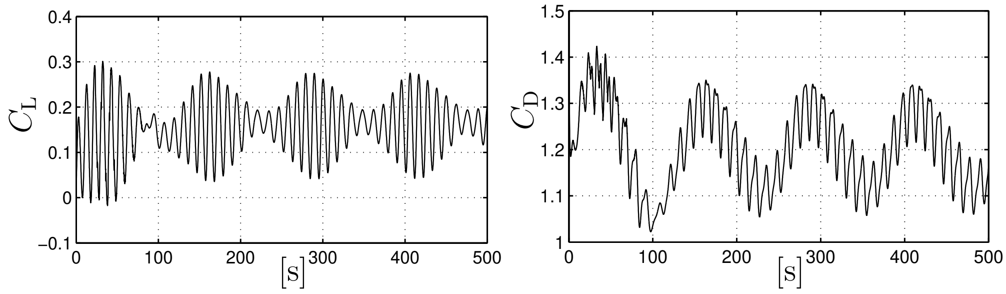

FIGURE 8. Lift (left) and drag (right) coefficients versus time for the cylinder connected to a vertical spring.

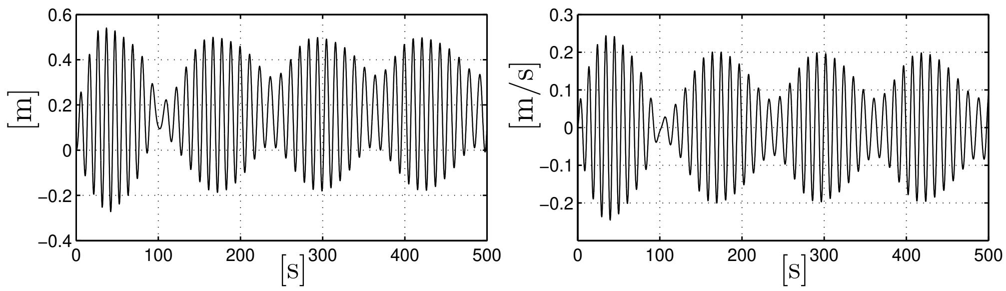

FIGURE 9. The vertical displacement (left) and the vertical velocity (right) of the cylinder connected to an elastic spring.

In order to retain a valid mesh, mesh smoothing has to be performed. In this example, standard Laplacian smoothing turned out not to be enough to provide a reasonable mesh due to crowding of nodes near Γ, see Figure 11. Instead we employed the more elaborate method proposed by Hermansson & Hansbo [11] (with the parameter p chosen as $p = 0.1$).

5. Concluding remarks

We have proposed a weak coupling method for solid-fluid interaction based on Nitsche's method. Since the coupling conditions are formulated in weak form, the approach can easily handle the case of non-matching meshes. In this paper, we have solved the problem globally coupled, but this is not necessary; the approach allows for any of the classical staggered iterative schemes to be invoked. From our point of view this is simply a question of efficiently solving the fully coupled problem.

We have merged the Nitsche approach with a space-time finite element method which we feel is the natural way of defining ALE methods (directly at the discrete level), and which also yields a simple way of formulating a Nitsche method for fluid-structure interaction. The space-time approach can be seen as a particular meshing of the space-time domain; it is the fact that the element sides are aligned with the "mesh velocity" that gives a close relation to classical ALE methods.

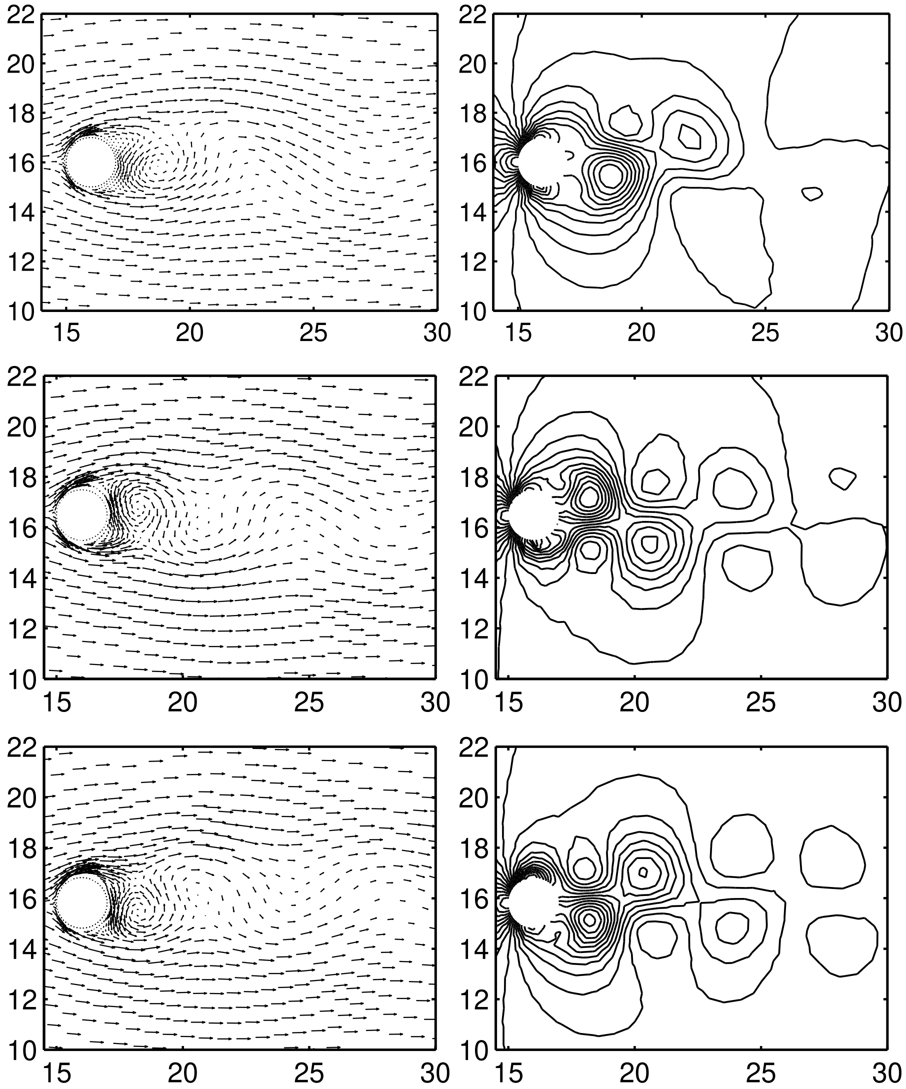

Figure 10. The velocity field when simulating the fluid-cylinder interaction. The velocity field (left) and the pressure (right). From top to bottom: Initial state, state when cylinder reaches maximum displacment at $t \approx 294$ [s] and the minimum cylinder displacement at $t \approx 299$ [s].

Examples have been given of the interaction between an incompressible fluid and a linearly elastic structure. Future work will focus on large deformation elasticity, in which case the fluid domain will change also due to the deformations of the solid domain.

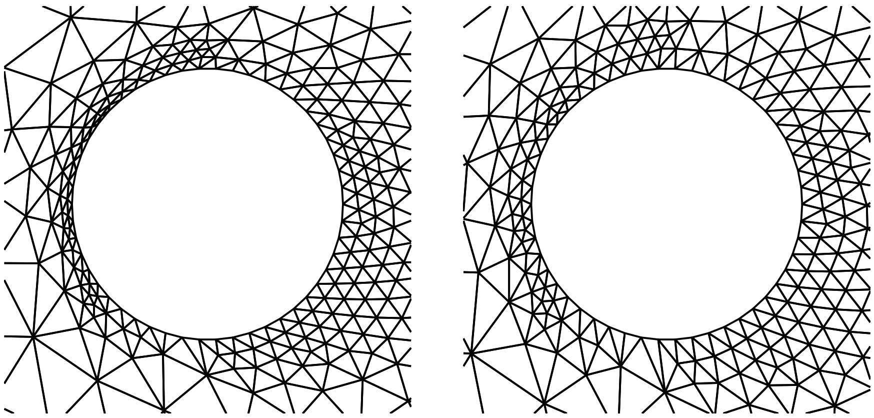

FIGURE 11. The mesh at maximum cylinder displacement ($t = 36.9\,[\mathrm{s}]$). The mesh smoothed using Laplacian smoothing (left) and the method proposed in [11] (with $p = 0.1$) (right).

References

[1] A. Alonso, A. Dello Russo, C. Otero-Souto, C. Padra, R. Rodríguez, An adaptive finite element scheme to solve fluid-structure vibration problems on non-matching grids, Comput. Visual. Sci. 4 (2001) 67–78.

[2] R. Becker, P. Hansbo, R. Stenberg, A finite element method for domain decomposition with non-matching grids, M2AN Math. Model. Numer. Anal. 37 (2003) 209–225

[3] F. Brezzi, M. Fortin, Mixed and Hybrid Finite Element Methods, Springer, Berlin, (1991).

[4] F. Casadei, J.P. Halleux, A. Sala, F. Chillè,Transient fluid-structure interaction algorithms for large industrial applications,Comput. Methods Appl. Mech. Eng. 190 (2001) 3081–3110

[5] C. Farhat, M. Lesoinne, P. LeTallec, Load and motion transfer algorithms for fluid/structure interaction problems with non-matching discrete interfaces: Momentum and energy conservation, optimal discretization and application to aeroelasticity, Comput. Methods Appl. Mech. Engrg. 157 (1998) 95–114.

[6] A. Hansbo, P. Hansbo, A finite element method for the simulation of strong and weak discontinuities in elasticity, Chalmers Finite Element Center Preprint 2003-09.

[7] P. Hansbo. The characteristic streamline diffusion method for the time-dependent incompressible Navier–Stokes equations. Comput. Methods Appl. Mech. Engrg., 99 (1992) 171–186.

[8] P. Hansbo, A Crank-Nicolson type space-time finite element method for computing on moving meshes, J. Comput. Phys. 159 (2000) 274–289.

[9] P. Hansbo, A note on energy conservation for Hamiltonian systems using continuous time finite elements, Commun. Numer. Methods Engrg. 17 (2001) 863–869.

[10] P. Hansbo, J. Hermansson, Nitsches method for coupling non-matching meshes in fluid-structure vibration problems, Comput. Mech. (to appear).

[11] J. Hermansson, P. Hansbo. A variable diffusion method for mesh smoothing, Comm. Numer. Methods Engrg. (to appear).

[12] E. Kuhl, S. Hulshoff, R. de Borst, An arbitrary Lagrangian Eulerian finite-element approach for fluid-structure interaction phenomena, Internat. J. Numer. Methods Engrg. 57 (2003) 117–142.

[13] H.G. Matthies, J. Steindorf,Partitioned but strongly coupled iteration schemes for nonlinear fluid-structure interaction,Comput. Struct. 80 (2002) 1991–1999.

[14] J. Nitsche, Über ein Variationsprinzip zur Lösung von Dirichlet-Problemen bei Verwendung von Teilräumen, die keinen Randbedingungen unterworfen sind. Abh. Math. Univ. Hamburg 36 (1971) 9–15.

[15] K.C. Park, C.A. Felippa, R. Ohayon, Partitioned formulation of internal fluid-structure interaction problems by localized Lagrange multipliers, Comput. Methods Appl. Mech. Engrg. 190 (2001) 2989–3007.

[16] B. Ramaswamy. Numerical Simulation of Unsteady Viscous Free Surface Flow. J. Comput. Phys., 90 (1990) 396–430.

[17] S. Mittal. T. E. Tezduyar. Notes on the stabilized space–time finite-element formulation of unsteady incompressible flows. Comput. Phys. Comm., 73 (1992) 93–112.

[18] J.J.W. van der Vegt and H. van der Ven. Space–time discontinuous Galerkin finite element method with dynamic grid motion for inviscid compressible flows. I. General formulation J. Comput. Phys., 182 (2002) 546–585.

Chalmers Finite Element Center Preprints

2001–01 *A simple nonconforming bilinear element for the elasticity problem*
Peter Hansbo and Mats G. Larson

2001–02 *The $\mathcal{LL}^*$ finite element method and multigrid for the magnetostatic problem*
Rickard Bergström, Mats G. Larson, and Klas Samuelsson

2001–03 *The Fokker-Planck operator as an asymptotic limit in anisotropic media*
Mohammad Asadzadeh

2001–04 *A posteriori error estimation of functionals in elliptic problems: experiments*
Mats G. Larson and A. Jonas Niklasson

2001–05 *A note on energy conservation for Hamiltonian systems using continuous time finite elements*
Peter Hansbo

2001–06 *Stationary level set method for modelling sharp interfaces in groundwater flow*
Nahidh Sharif and Nils-Erik Wiberg

2001–07 *Integration methods for the calculation of the magnetostatic field due to coils*
Marzia Fontana

2001–08 *Adaptive finite element computation of 3D magnetostatic problems in potential formulation*
Marzia Fontana

2001–09 *Multi-adaptive galerkin methods for ODEs I: theory & algorithms*
Anders Logg

2001–10 *Multi-adaptive galerkin methods for ODEs II: applications*
Anders Logg

2001–11 *Energy norm a posteriori error estimation for discontinuous Galerkin methods*
Roland Becker, Peter Hansbo, and Mats G. Larson

2001–12 *Analysis of a family of discontinuous Galerkin methods for elliptic problems: the one dimensional case*
Mats G. Larson and A. Jonas Niklasson

2001–13 *Analysis of a nonsymmetric discontinuous Galerkin method for elliptic problems: stability and energy error estimates*
Mats G. Larson and A. Jonas Niklasson

2001–14 *A hybrid method for the wave equation*
Larisa Beilina, Klas Samuelsson and Krister Åhlander

2001–15 *A finite element method for domain decomposition with non-matching grids*
Roland Becker, Peter Hansbo and Rolf Stenberg

2001–16 *Application of stable FEM-FDTD hybrid to scattering problems*
Thomas Rylander and Anders Bondeson

2001–17 *Eddy current computations using adaptive grids and edge elements*
Y. Q. Liu, A. Bondeson, R. Bergström, C. Johnson, M. G. Larson, and K. Samuelsson

2001–18 *Adaptive finite element methods for incompressible fluid flow*
Johan Hoffman and Claes Johnson

2001–19 *Dynamic subgrid modeling for time dependent convection–diffusion–reaction equations with fractal solutions*
Johan Hoffman

2001–20 *Topics in adaptive computational methods for differential equations*
Claes Johnson, Johan Hoffman and Anders Logg

2001–21 *An unfitted finite element method for elliptic interface problems*
Anita Hansbo and Peter Hansbo

2001–22 *A P^2–continuous, P^1–discontinuous finite element method for the Mindlin-Reissner plate model*
Peter Hansbo and Mats G. Larson

2002–01 *Approximation of time derivatives for parabolic equations in Banach space: constant time steps*
Yubin Yan

2002–02 *Approximation of time derivatives for parabolic equations in Banach space: variable time steps*
Yubin Yan

2002–03 *Stability of explicit-implicit hybrid time-stepping schemes for Maxwell's equations*
Thomas Rylander and Anders Bondeson

2002–04 *A computational study of transition to turbulence in shear flow*
Johan Hoffman and Claes Johnson

2002–05 *Adaptive hybrid FEM/FDM methods for inverse scattering problems*
Larisa Beilina

2002–06 *DOLFIN - Dynamic Object oriented Library for FINite element computation*
Johan Hoffman and Anders Logg

2002–07 *Explicit time-stepping for stiff ODEs*
Kenneth Eriksson, Claes Johnson and Anders Logg

2002–08 *Adaptive finite element methods for turbulent flow*
Johan Hoffman

2002–09 *Adaptive multiscale computational modeling of complex incompressible fluid flow*
Johan Hoffman and Claes Johnson

2002–10 *Least-squares finite element methods with applications in electromagnetics*
Rickard Bergström

2002–11 *Discontinuous/continuous least-squares finite element methods for elliptic problems*
Rickard Bergström and Mats G. Larson

2002–12 *Discontinuous least-squares finite element methods for the Div-Curl problem*
Rickard Bergström and Mats G. Larson

2002–13 *Object oriented implementation of a general finite element code*
Rickard Bergström

2002-14 *On adaptive strategies and error control in fracture mechanics*
Per Heintz and Klas Samuelsson

2002-15 *A unified stabilized method for Stokes' and Darcy's equations*
Erik Burman and Peter Hansbo

2002-16 *A finite element method on composite grids based on Nitsche's method*
Anita Hansbo, Peter Hansbo and Mats G. Larson

2002-17 *Edge stabilization for Galerkin approximations of convection–diffusion problems*
Erik Burman and Peter Hansbo

2002-18 *Adaptive strategies and error control for computing material forces in fracture mechanics*
Per Heintz, Fredrik Larsson, Peter Hansbo and Kenneth Runesson

2002-19 *A variable diffusion method for mesh smoothing*
J. Hermansson and P. Hansbo

2003-01 *A hybrid method for elastic waves*
L.Beilina

2003-02 *Application of the local nonobtuse tetrahedral refinement techniques near Fichera-like corners*
L.Beilina, S.Korotov and M. Křížek

2003-03 *Nitsche's method for coupling non-matching meshes in fluid-structure vibration problems*
Peter Hansbo and Joakim Hermansson

2003-04 *Crouzeix–Raviart and Raviart–Thomas elements for acoustic fluid–structure interaction*
Joakim Hermansson

2003-05 *Smoothing properties and approximation of time derivatives in multistep backward difference methods for linear parabolic equations*
Yubin Yan

2003-06 *Postprocessing the finite element method for semilinear parabolic problems*
Yubin Yan

2003-07 *The finite element method for a linear stochastic parabolic partial differential equation driven by additive noise*
Yubin Yan

2003-08 *A finite element method for a nonlinear stochastic parabolic equation*
Yubin Yan

2003-09 *A finite element method for the simulation of strong and weak discontinuities in elasticity*
Anita Hansbo and Peter Hansbo

2003-10 *Generalized Green's functions and the effective domain of influence*
Donald Estep, Michael Holst, and Mats G. Larson

2003-11 *Adaptive finite element/difference method for inverse elastic scattering waves*
L.Beilina

2003-12 *A Lagrange multiplier method for the finite element solution of elliptic domain decomposition problems using non-matching meshes*
Peter Hansbo, Carlo Lovadina, Ilaria Perugia, and Giancarlo Sangalli

2003-13 *A reduced P^1–discontinuous Galerkin method*
Roland Becker, Erik Burman, Peter Hansbo and Mats G. Larson

2003-14 *Nitsche's method combined with space–time finite elements for ALE fluid–structure interaction problems*
Peter Hansbo, Joakim Hermansson, and Thomas Svedberg

These preprints can be obtained from

`www.phi.chalmers.se/preprints`